Magnetism of nanocrystalline $(La_{0.5}Sr_{0.5})TiO_3$ doped with 3d cations

2010 J. Phys.: Condens. Matter 22 096004

(http://iopscience.iop.org/0953-8984/22/9/096004)

J. Phys.: Condens. Matter **22** (2010) 096004 (9pp) doi:10.1088/0953-8984/22/9/096004

Magnetism of nanocrystalline $(La_{0.5}Sr_{0.5})TiO_3$ doped with 3d cations

Kwanruthai Wongsaprom[1,2], M Venkatesan[1], Santi Maensiri[2] and J M D Coey[1]

[1] CRANN and School of Physics, Trinity College, Dublin 2, Republic of Ireland
[2] Department of Physics, Khon Kaen University, Khon Kaen 40002, Thailand

Received 10 July 2009, in final form 30 November 2009
Published 10 February 2010
Online at stacks.iop.org/JPhysCM/22/096004

Abstract

Nanocrystallites of nominal composition $(La_{0.5}Sr_{0.5})TiO_3$ 12–15 nm in diameter exhibit a diamagnetic susceptibility that is greater by a factor of three than that of bulk ceramic material, due to a much-reduced Pauli paramagnetic contribution associated with oxidation (cation deficiency) of the material. Doping the nanocrystallites with 1.5 or 2.0% of every transition metal from V–Ni adds a Curie term to the susceptibility. Exchange coupling between these paramagnetic ions is very weak. In the cases of Fe, Co and Ni there is an additional hysteretic ferromagnetic magnetization, with a moment equivalent to a few tenths of a Bohr magneton per dopant atom, which is attributed to a secondary ferromagnetic impurity phase. Mössbauer analysis of samples prepared with ^{57}Fe reveals the presence of some metallic iron. Metallic nickel is detected by x-ray diffraction, but no direct evidence of metallic cobalt was found in the ferromagnetic Co-doped material. The possibility of high temperature defect-related ferromagnetism in a metallic oxide is discussed.

(Some figures in this article are in colour only in the electronic version)

1. Introduction

Dielectric oxides doped with a small amount of 3d transition metal ions are a puzzling and controversial group of magnetic materials. Interest in them was sparked by a report from Matsumoto *et al* in 2001 [1] that thin films of TiO_2 doped with 7% of Co ions were ferromagnetic at room temperature. Recent reviews [2–5] summarize much of the work on oxides such as ZnO, TiO_2, SnO_2, HfO_2, CeO_2, In_2O_3 and $SrTiO_3$ doped with 1–5% of metals such as V, Mn, Fe, Co and Ni. The magnetic samples are usually in thin film form, but there are also reports of room temperature ferromagnetism in doped nanoparticles and nanocrystallites. Examples include ZnO [6–10], SnO_2 [11–15], TiO_2 [16] and CeO_2 [17]. In some cases, undoped nanoparticles [9, 18] have been reported to be ferromagnetic. Other studies, for example that of Bérardan *et al* [19] on In_2O_3, find that nanoparticles prepared in a variety of different conditions are completely diamagnetic and transition-metal-doped samples are paramagnetic.

The characteristic signature of the high temperature ferromagnetism is that it is anhysteretic, with magnetization curves of the approximate form:

$$M \approx M_s \tanh(H/H_0) \quad (1)$$

where M_s and H_0 are values that are essentially independent of temperature below room temperature. H_0 often lies in the range 60–120 kA m^{-1}, but M_s varies greatly, in a manner that is often irreproducible. Values of magnetization of order 10 kA m^{-1} are found in some doped nanoparticles, but M_s can depend on the state of aggregation of the particles [6, 16, 20]; the values in undoped nanoparticles with a crystallite size $\leqslant$20 nm are much smaller, $\leqslant$10 A m^{-1} (0.01 emu cm^{-3}) [18]. The magnetism seems to be associated with electrons in surface or defect states, such as grain boundaries [9], rather than the ions in the lattice. A recent analysis of the magnetization curves based on the assumption that they are determined by dipolar interactions shows that only a small fraction of the volume of these materials is actually ferromagnetically ordered [21].

Well-crystallized bulk samples [22, 23] and thin films [24] of dilute magnetic oxides behave as expected—they are paramagnetic down to the helium temperature range. When a few per cent of 3d dopants are distributed at random on the cation sites, the expectations are clear. Isolated ions are paramagnetic. Pairs and small clusters of ions will form statistically. The coupling between pairs of magnetic ions which share an oxygen bridge is superexchange, which is usually antiferromagnetic, and a

Curie–Weiss susceptibility is the result. Small clusters will also give rise to a Curie–Weiss-like contribution to susceptibility. The anticipated paramagnetic behaviour is normally observed in well-crystallized dilute magnetic oxides [22–24]. Small concentrations of conduction electrons do provide ferromagnetic coupling [25] but the carrier-mediated interaction between impurities is only a few kelvin. An estimate of the magnitude of the magnetic-ordering temperature due to the RKKY interaction is

$$T_C = 2ZJS(S+1)/3k_B \quad (2)$$

with $J \propto J_{sd}^2 F(\xi)$ [26]. Here, Z is the number of interacting neighbours and $F(\xi)$ is the RKKY function. The Curie temperature at elevated carrier concentrations, corresponding to about 10^{21} cm^{-3}, does not exceed a few tens of kelvin [1, 2] which is too low by one or two orders of magnitude to account for the high temperature ferromagnetism. If we relax the assumption of a random distribution of magnetic impurities, and admit that they are somehow segregated in clusters or planar regions that result, for example, from spinodal decomposition, it is possible to increase T_c, but then one runs into another problem. Small clusters will be superparamagnetic. The magnetization curves described by (1), although almost anhysteretic, show no sign of the characteristic feature of superparamagnetism, which is scaling of the magnetization as a function of H/T—the argument of the Langevin function is (H/T). In fact, the magnetization curves are remarkably independent of temperature in these systems.

Here, we are interested in the behaviour of magnetic impurities doped into a host which is neither an insulator nor a normal metal. Well-crystallized $(La_{0.5}Sr_{0.5})TiO_3$ (abbreviated here as LSTO) is a d-band metal. Oxygen-stoichiometric samples prepared by annealing $SrTiO_3$ and $LaTiO_3$ crystallize in an orthorhombically distorted perovskite-type cell, space group $Ibmm$ with $a = 0.5573$, $b = 0.5342$ and $c = 0.7827$ nm. The lattice parameter for the corresponding undistorted cubic cell is $a_0 \approx 0.392$ nm. Susceptibility is paramagnetic and temperature-independent $\chi_{mol} = 0.94 \times 10^{-9}$ m^3 mol^{-1}, and resistivity is 10^{-2} Ω m, with a metallic temperature dependence [27]. Single crystals are reported [28] to have a susceptibility (after correction for core diamagnetism) of 1.75×10^{-9} m^3 mol^{-1} and an electronic specific heat coefficient $\gamma = 5$ mJ mol^{-1} K^2, both of which are consistent with a density of states at the Fermi level of 2.1 states eV^{-1} formula^{-1}. The occupied d bandwidth is therefore about 0.2 eV wide.

An insulator–metal transition occurs in the $(La_{1-x}Sr_x)TiO_3$ solid solution at $x = 0.05$. The end member $LaTiO_3$ is a canted antiferromagnet, with localized Ti^{3+} ions ($S = 1/2$), but oxides with $x > 0.05$ are Pauli paramagnets [28]. The electronic properties of LSTO are quite sensitive to oxygen stoichiometry. Samples range from black metals to white insulators. On increasing x in $(La_{1-x}Sr_x)TiO_3$, the Ti d-band will be emptied at $x = 1$, but if the compound is nonstoichiometric, it is expected to become insulating when LSTO is oxidized (cation-deficient) to the extent $\delta = 0.077$ in the formula $(La_{0.5}Sr_{0.5}Ti)_{1-\delta}O_3$.

First reports of high temperature ferromagnetism in LSTO were for Co-doped thin films by Zhao *et al* [29]. Oxygen-deficient films with $x = 1.5\%$ prepared by pulsed-laser deposition exhibited moments of up to 2.6 μ_B/Co and a Curie temperature of 450 K. Moments of 1.7 μ_B/Co were measured in films grown on different substrates by another group [30]. By incorporating these films into magnetic tunnel junctions, it was possible to infer a high spin polarization of 80% for the Co-LSTO dilute ferromagnetic oxide.

In an earlier report by Wongsaprom *et al*, it was shown that a large ferromagnetic magnetization may also be observed in Co-LSTO nanocrystallites [31]. Here, we follow with systematic investigation of the magnetic properties of LSTO, undoped and with transition metal doping (substitution for Ti at the 1.5 or 2.0% level) for dopants ranging from Sc to Ni. Our samples are usually in nanocrystalline form. We include some Mössbauer spectra of ^{57}Fe-doped materials and compare undoped ceramic and nanocrystalline material. Finally, we discuss the origins of the magnetism in these materials.

2. Experimental methods

$(La_{0.5}Sr_{0.5})TiO_3$ nanoparticles, approximately 12–15 nm in diameter, were synthesized by a polymerized complex method, which has been used to synthesize polycation oxide powders, using Ti isopropoxide and nitrate precursors, with citric acid and ethylene glycol [31, 32]. A hydrocarboxylic acid, such as citric acid, was used to chelate cations in aqueous solution. The addition of a glycol, such as ethylene glycol, leads to organic ester formation. Polymerization, promoted by heating the mixture, results in a homogeneous resin in which metal ions are uniformly distributed throughout the organic matrix. The resin was then calcined at 350 °C for 1 h (primary calcination), leading to the partial decomposition of some organics. The resultant material of the primary calcination was ground to give a brown powder. The brown powders of LSTO with and without transition metal doping were then calcined under flowing argon at 930 °C for 2 h. Undoped samples, and samples doped with a nominal concentration of 1.5% or 2% of elements of the 3d series from Sc–Ni, were prepared. All the final materials are black nanocrystalline powders.

Bulk ceramic samples of undoped LSTO, and LSTO with 2% ^{57}Fe doping, were made by mixing and firing the components at 1000 °C. 2 g of powder was ground and pressed into a pellet of 13 mm diameter in a hydraulic press. The pellet was then placed in a ceramic boat and sintered at 1150 °C for 24 h in air or flowing argon. Nominal purity of the starting materials was 99.99% or better. The mixing and grinding processes were carried out in an agate mortar and pestle which was cleaned thoroughly before and after use with aqua regia. The ceramic samples were grey or yellowish in colour. They were not electrically conducting.

Crystal structure measurements were performed using a Philips x-ray diffractometer. Scanning electron microscopy (SEM) and energy dispersive x-ray analysis (EDAX) was used for elemental analysis and mapping. Magnetization measurements were made in a SQUID magnetometer at both 300 and 5 K, and thermal scans of the magnetization in a 1 T

Table 1. Properties of $(La_{0.5}Sr_{0.5})TiO_3$.

Sample	Heat treatment	Lattice parameter (nm)	Colour	χ_0 ($m^3\ kg^{-1}$ (10^{-9}))	y (%)
Ceramic	1150 °C in argon	0.3882	Yellow	−1.2	0.04
Nanocrystalline powder	930 °C in argon	0.3925	Dark grey	−4.1	0.62

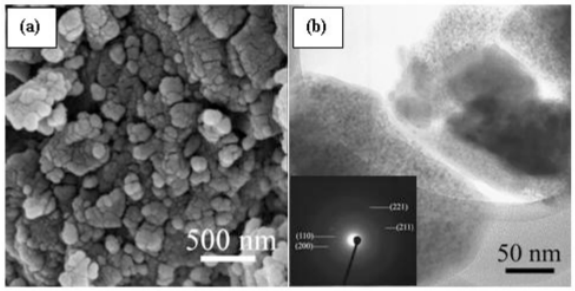

Figure 1. (a) SEM micrograph and (b) TEM bright-field image with corresponding selected-area electron diffraction (SAED) patterns (insets) of nanocrystalline LSTO samples.

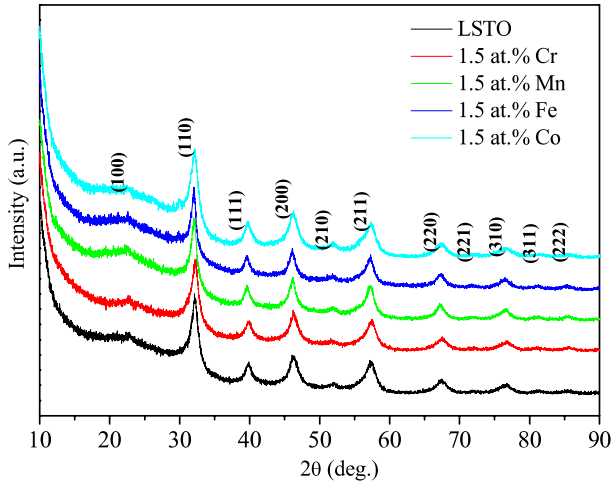

Figure 2. XRD patterns of LSTO and 1.5 at.% of Cr-, Mn-, Fe-and Co-doped LSTO samples.

field were carried out from 5 to 300 K. Powder samples were mounted in gel caps, which have a temperature-independent diamagnetic susceptibility of -5.9×10^{-9} $m^3\ kg^{-1}$ and the gel caps were placed in drinking straws for the measurement. Ceramic samples were mounted directly in the drinking straws. Mössbauer data for samples made with natural iron or ^{57}Fe were collected in the transmission mode on a standard constant-acceleration spectrometer with a $^{57}Co/Rh$ source.

3. Results

3.1. LSTO

First, we characterize the host LSTO material. Properties of nanocrystalline and ceramic material are summarized in table 1. Scanning electron micrographs are shown in figure 1. The average crystallite size is about 12 nm and the crystallites are agglomerated into larger masses. The x-ray diffraction data in figure 2 for the nanocrystalline material shows a pattern which can be indexed as a cubic perovskite with $a_0 = 0.3925$ nm. From the line broadening, the crystallite size D was estimated using the Scherrer formula $D = 0.89\lambda/(\beta \cos\theta)$, where λ is the wavelength of the x-ray radiation, θ is the diffraction angle and β is the full width at half-maximum of the broadening. A crystallite size of 12–15 nm is deduced in this way.

The room temperature magnetization curve for a nanocrystalline sample is shown in figure 3(a), including the gel cap sample holder. The curve is linear and diamagnetic, with no trace of ferromagnetic behaviour. After correction for the diamagnetism of the sample holder, the susceptibility for the grey nanocrystalline material is deduced as $\chi_{dia} = -4.1 \times 10^{-9}$ $m^3\ kg^{-1}$. Figure 3(b) shows the temperature dependence of magnetization in 1 T of an empty gel cap, together with data for a nanocrystalline powder and a ceramic sample. The ceramic is yellowish in colour and insulating. It has considerably less diamagnetic susceptibility $\chi_{dia} = -1.2 \times 10^{-9}$ $m^3\ kg^{-1}$. Both LSTO materials exhibit an upturn in the magnetization at low temperature, which depends on thermal treatment. The upturn is greater in oxygen-deficient samples, annealed in argon, than it is for samples annealed in air. The susceptibility is fitted as the sum of a temperature-independent term χ_0 (which is the sum of the core diamagnetic and Pauli paramagnetic terms) and a temperature-dependent, Curie–Weiss term $\chi_{CW} = \mu_0 n y g^2 \mu_B^2 S(S+1)/3k_B(T-\theta) = \mu_0 y p_{eff}^2/3k_B(T-\theta)$, where n is the number of localized moments with spin S:

$$\chi = \chi_0 + \chi_{CW}. \tag{3}$$

This procedure gives atomic concentrations of paramagnetic spin-1/2 defects of $y = 0.62\%$ and $y = 0.04\%$ for the nanocrystalline and ceramic samples, respectively. In both cases the paramagnetic Curie temperature θ was close to zero.

The differences between the ceramic and nanocrystalline host material are significant. The ceramics show a diamagnetic susceptibility that is smaller by a factor of three than that of the nanoparticles. Expressed as a molar susceptibility, the susceptibility is $\chi_{mol} = -0.26 \times 10^{-9}$ for the ceramics prepared in air and $\chi_{mol} = -0.86 \times 10^{-9}$ for the nanoparticles. Different batches of nanoparticles gave susceptibilities that varied by about 20%.

The purpose of presenting the uncorrected raw data in figure 3, is to show that it is quite possible for the sign of the moment of a ceramic sample, or a nanocrystalline powder and its sample holder, to change sign as a function of temperature if it is doped with paramagnetic ions. When

Table 2. Analysis of the paramagnetic susceptibility of LSTO. (Note: is low spin.)

Dopant	Nominal concentration (%)	Corrected nominal concentration (%)[a]	χ (m^3 kg^{-1}) 10^{-9}	C_{mol} (m^3 mol^{-1}) 10^{-9}	θ (K)	P_{eff} (μ_B)	Possible valence	Corresponding P_{eff} (μ_B)
Sc	1.5	1.5	−3.9	8.7	—	0.6	Sc^{2+}	1.7
V	1.5	1.5	−3.3	25	−4	1.0	V^{4+}	1.7
Cr	15	1.5	−1.0	161	0	2.5	Cr^{3+}	3.9
Mn	1.5	1.5	1.7	400	−1	3.9	Mn^{4+}	3.9
Fe	2.0	1.6		128	−25	2.3	Fe^{2+}	4.9
Fe[b]	2.0	2.0	0.8	831	−3	5.2	Fe^{3+}	5.9
Co	2.0	1.4		68	1	1.9	Co^{2+} (ls)	1.7
Ni	1.5	1.1		77	−12	1.6	Ni^{+}	1.7

[a] Corrected for the fraction of magnetically ordered dopant ions (assuming the metallic moment).
[b] Ceramic sample.

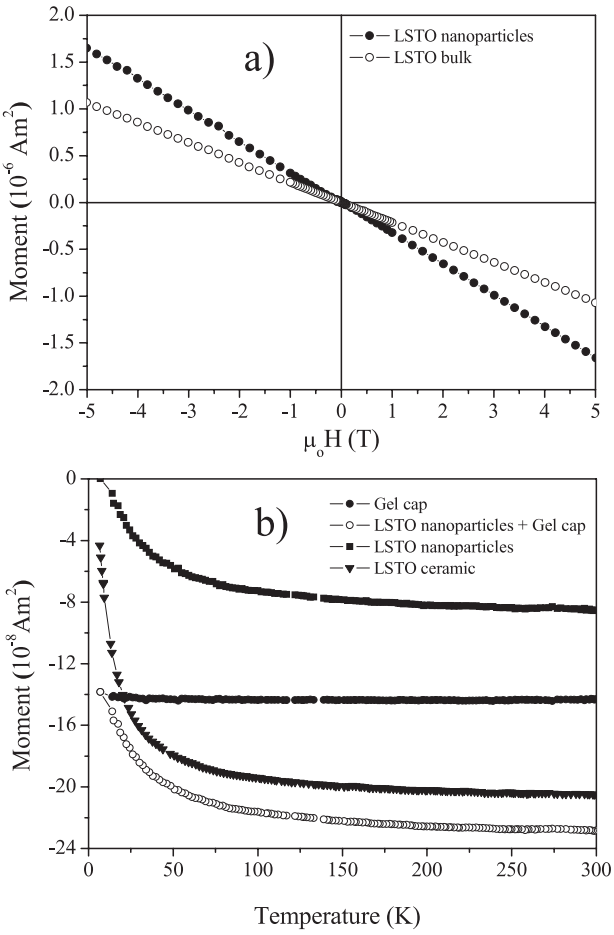

Figure 3. (a) Magnetization curve of nanocrystalline LSTO powder in a gel cap sample holder, with the curve for a blank sample holder. (b) Thermal scans of magnetization in 1 T for the LSTO powder in the gel cap, the gel cap alone and the difference (it is compared with the signal from a ceramic sample, which is not mounted in a gel cap).

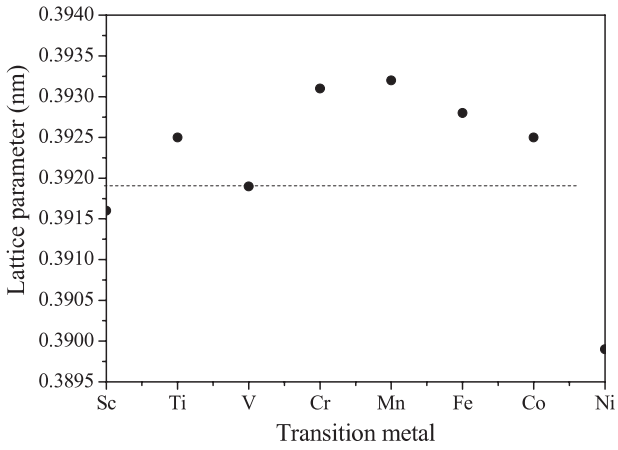

Figure 4. Lattice parameters for the series of doped LSTO nanocrystals.

an iterative regression procedure is used in the SQUID magnetometer with sample position tracking, incorrect values of total magnetic moment are extracted at temperatures close to that where the dipole component of the sample magnetic moment changes sign. A sharp change of the moment versus temperature signal is recorded which resembles the variation near a phase transition, but it is actually an artefact of the measuring technique. To avoid these problems, it is best either to measure a set of isothermal magnetization curves at different temperatures or to construct a sample mounting with a sufficiently small diamagnetic contribution in order to ensure the total dipole magnetic moment does not change sign during the measurement.

3.2. Doped LSTO

The XRD patterns of some doped LSTO samples were shown in figure 2. They are similar to that of the undoped LSTO. There is no signature of secondary phases, with the sole exception of the Ni-doped sample, where the face-centred cubic Ni(111) reflection could be seen (not shown). Lattice parameters for the series are plotted in figure 4. Crystallite sizes were estimated from the Scherrer formula and values of 6–14 nm were found.

The samples doped with cations from Sc–Mn all exhibit linear magnetization curves and a Curie–Weiss susceptibility superposed on the temperature-independent term (equation (2)). The analysis of the data is summarized in table 2 for the dopants from V to Ni. Values of χ_0 are included for all the materials which show linear magnetization curves. The concentrations of localized impurities $S = 1/2$ in the Sc and Ti (undoped) materials are 0.1% and 0.6%,

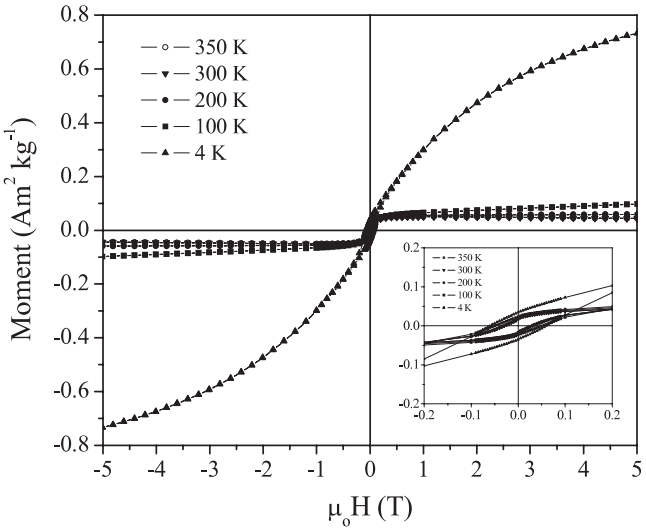

Figure 5. Magnetization curves for a 2 at.% ^{57}Fe-doped LSTO sample at temperatures ranging from 4 to 350 K.

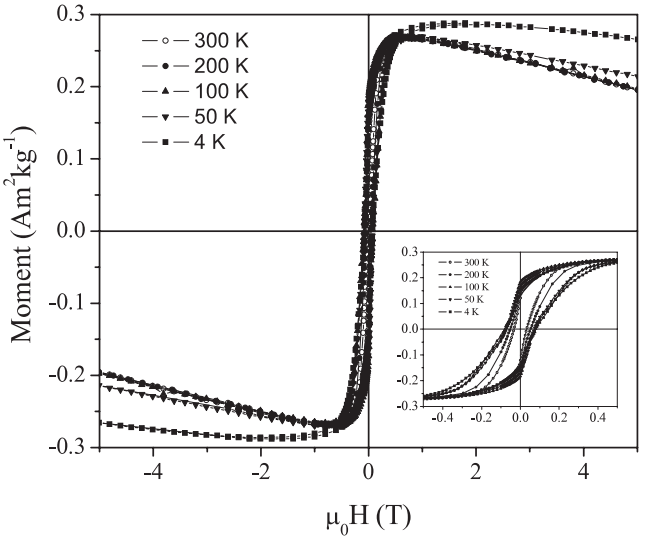

Figure 6. Magnetization curves as a function of temperature for Co-doped samples with $x = 0.02$.

Table 3. Ferromagnetic moments per dopant cation for LSTO nanoparticles.

	σ (A m^2 kg^{-1})	σ (A m^2 kg^{-1} of TM)	m (μ_B per TM)
Fe	0.10	19	0.19
Co	0.30	53	0.53
Ni	0.06	14	0.14

respectively, and the values of χ_0 are -1.8×10^{-9} m^3 kg^{-1} and -5.1×10^{-9} m^3 kg^{-1}, respectively.

The nanocrystalline samples doped with the late transition elements Fe, Co and Ni behave differently. In addition to a temperature-dependent, Curie–Weiss term in the susceptibility, they all show a nonlinear, ferromagnetic-like component in their magnetization curves that exhibit temperature-dependent hysteresis with a remanence ratio of 0.2–0.7 (figures 5–7). The measured moments, which are a few tenths of a Bohr magneton per dopant atom, are summarized in table 3. The paramagnetic and ferromagnetic moments, together with Curie temperatures estimated by extrapolation of the ferromagnetic moment, are plotted in figure 8. The ferromagnetism could be due to nanoscale inclusions of the transition metals, although only in the case of nickel is there direct x-ray evidence of this. Alternatively, it might be an intrinsic property of the doped LSTO, although temperature-dependent hysteresis with a large remanence is not the behaviour described by (1). In order to investigate this further, we prepared ceramic and nanocrystalline samples doped with 1.5% of natural iron or 2.0% of ^{57}Fe for Mössbauer spectroscopy.

In the first case, a correction was made for the Mössbauer absorption due to the iron in the window of the proportional counter. The main absorption peaks are a narrow quadruple doublet with an isomer shift, relative to αFe, of 0.38 mm s^{-1}, which is associated with Fe^{3+} ions in almost undistorted octahedral sites of the perovskite structure, and a large quadruple doublet with isomer shift of 0.84 mm s^{-1} and quadrupole splitting of 1.71 mm s^{-1}, which is associated with Fe^{2+} in the same sites [33].

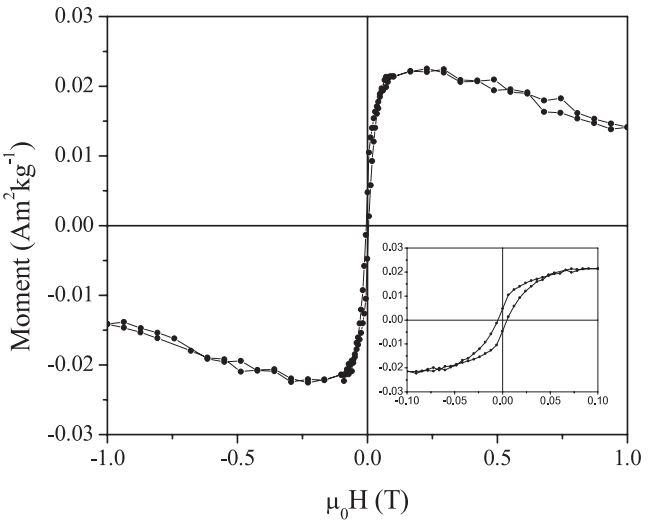

Figure 7. Room temperature magnetization curve Ni-doped sample with $x = 0.02$.

In the case of the ceramic sample, which shows a purely linear, paramagnetic magnetization curve with no trace of ferromagnetism, only the narrow ferric quadrupole doublet is seen (figure 9(a)). However, in the spectrum of the nanocrystalline ^{57}Fe sample, the paramagnetic doublets coexist with some weak magnetically split hyperfine structure (figure 9(b)). Magnetic hyperfine patterns with $B_{hf} = 46.9$ T or 33.0 T are resolved, which are associated with magnetically ordered Fe^{3+} and metallic iron, respectively. Almost 3% of the iron dopant is in the metallic form.

4. Discussion

4.1. LSTO

The electronic and magnetic properties of $La_{0.5}Sr_{0.5}TiO_3$ are governed by the triply-degenerate t_{2g} bands of titanium.

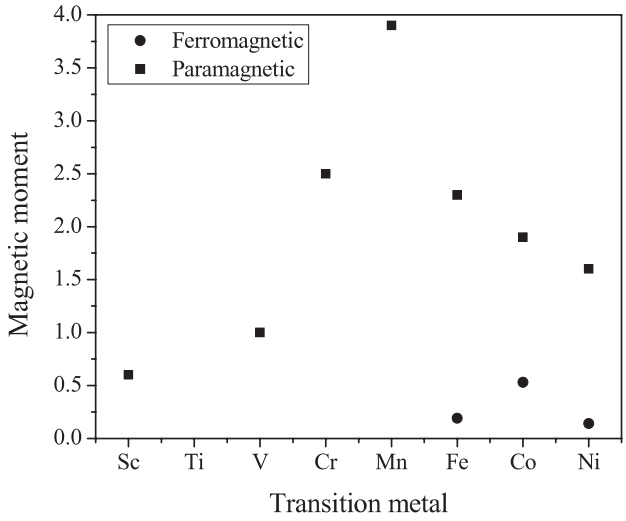

Figure 8. Paramagnetic and ferromagnetic moments for different transition metal doping. The paramagnetic moment ■ is p_{eff} per paramagnetic ion; the ferromagnetic moment ● is m per dopant atom.

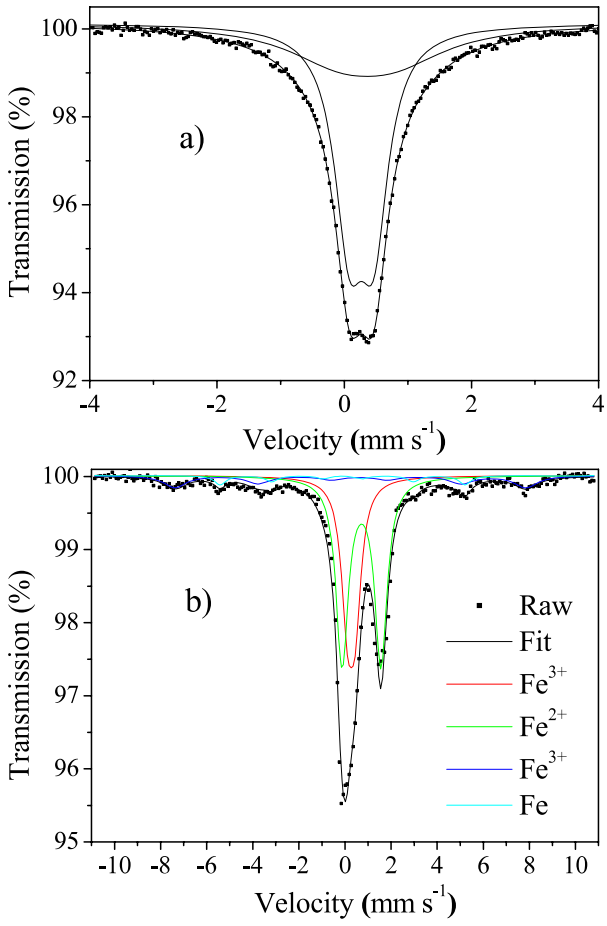

Figure 9. ^{57}Fe Mössbauer spectra of (a) a ceramic sample of Fe-doped LSTO and (b) a nanocrystalline sample of Fe-doped LSTO.

The end member $LaTiO_3$, when well prepared, is a Mott–Hubbard insulator, although in the literature it is sometimes characterized as a correlated or a poor metal. At high

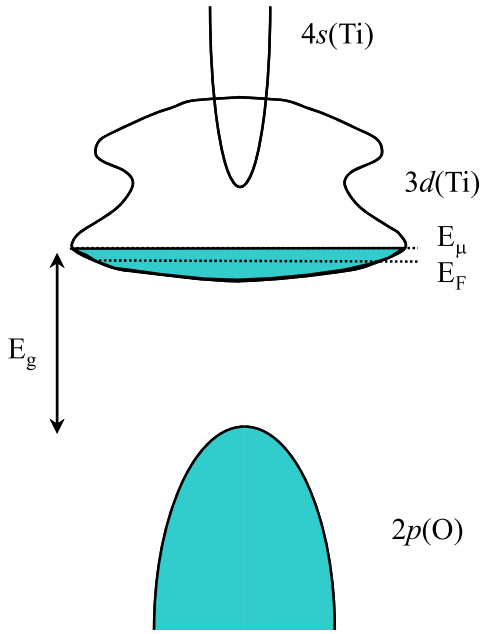

Figure 10. Electronic structure of LSTO. The bandgap $E_g = 3.8$ eV is deduced from the optical absorption edge. E_F is the Fermi energy and E_μ is the mobility edge.

temperature this material is paramagnetic. The other end member $SrTiO_3$ is an uncorrelated band insulator with a direct gap $E_g = 3.3$ eV. In this picture, the Ti d-band of $La_{0.5}Sr_{0.5}TiO_3$ contains 0.5 electrons formula^{-1}, which occupy states at the bottom of the narrow t_{2g} sub-band, which has six states per Ti. The difference in susceptibility between the core diamagnetism for the ions in LSTO ($\chi_{\text{mol}} = -0.73 \times 10^{-9}$ m^3 mol^{-1}) [34] and the susceptibility observed for bulk ceramic samples ($\chi_{\text{mol}} = -0.26 \times 10^{-9}$ m^3 mol^{-1}) is 0.47×10^{-9} m^3 mol^{-1}, identified as the Pauli paramagnetism of this band. This estimate may be compared with that of Tokura *et al* who found a considerably larger Pauli susceptibility for a single crystal, ($\chi_{\text{mol,Pauli}} = 1.4 \times 10^{-4}$ emu mol^{-1}, which is equivalent to 1.75×10^{-9} m^3 mol^{-1}, or a dimensionless susceptibility of 48×10^{-6}). The expression for the dimensionless Pauli susceptibility is

$$\chi_{\text{Pauli}} = 2\mu_0\mu_B^2 N(E_F). \tag{4}$$

In the free-electron model $N(E_F) = 3n/4E_F$, where n is the electron density in the band. Assuming stoichiometry, the 0.5 electrons (formula unit)$^{-1}$ corresponds to $n = 8.3 \times 10^{27}$ m^{-3}, which gives an occupied bandwidth of 0.17 eV for the Ti t_{2g} band, which is a plausible value. The total t_{2g} bandwidth is then 2.1 eV. The schematic electronic density of states for LSTO is illustrated in figure 10.

In the free-electron model, $\chi_{\text{Pauli}} \propto n^{1/3}$. The smaller Pauli susceptibility in our ceramic samples indicates that they are nonstoichiometric, with $n \approx 0.2 \times 10^{27}$ m^{-1}, or 0.01 conduction electrons per formula unit. The occupied bandwidth is only 13 meV. The black nanocrystalline material has a diamagnetic susceptibility $\chi_{\text{mol}} = -0.86 \times 10^{-9}$ m^3 mol^{-1}, which is similar to the core diamagnetism

Table 4. Mössbauer hyperfine parameters.

Dopant	x (%)	Sample		δ (mm s^{-1})	Area (%)	Δ (mm s^{-1})	B_{hf} (T)
Fe	1.5	Nanoparticles	Fe^{2+}	0.270	62.5	0.279	—
			Fe^{3+}	0.375	37.5	1.016	—
^{57}Fe	2.0	Nanoparticles	Fe^{2+}	0.713	57.7	1.661	—
			Fe^{3+}	0.350	21.5	−0.241	—
			Fe^{3+}	0.398	18.1	−0.206	46.9
			Iron	−0.106	2.7	0.000	33.0
^{57}Fe	2.0	Ceramic	Fe^{3+}	−0.202	100	0.000	—

$\chi_{mol,core} = -0.73 \times 10^{-9}$ m^3 mol^{-1}. There appear to be *few* conduction electrons in the nanocrystalline LSTO, which implies a cation deficiency close to $\delta = 0.077$. The values of χ_0 for the doped LSTO nanoparticles listed in table 2 are quite variable, but in all cases greater than for the undoped material. This indicates that the titanium d-band is filled to different extents for the different dopings.

At this point the potential fluctuations created at the Ti sites by the randomly placed La^{3+} and Sr^{2+} cations should be considered. Unscreened, these fluctuations will be $\Delta V = e/4\pi\varepsilon_0\varepsilon r$, or about 0.4 eV, using $\varepsilon \approx 10$ and $r = 0.34$ nm as the La–Ti distance. Even when screened, they may be comparable to the occupied bandwidth, creating a mobility edge [35], as illustrated in figure 10. States at the bottom of the titanium d-band are localized. The Fermi level lies above the mobility edge for well-crystallized, stoichiometric metallic LSTO with 0.5 conduction electrons per formula. The material is a metal, but as the d-band is emptied, the electrons settle into localized states as the Fermi level falls below the mobility edge. This explains why our ceramic samples of LSTO produced in oxidized and reduced conditions, as well as the nanocrystalline LSTO, are actually insulating. The susceptibility of these localized d-band states is expected to be Pauli-like rather than Curie-like when the localization length is long compared with the interatomic spacing.

The nanocrystals naturally have a high density of surface and interface states. Approximately 10% of the Ti cations are at the surface. The small Curie-like upturn of the susceptibility visible below 10 K in the undoped LSTO in figure 3(b) is attributed to a small number of Ti^{3+} ions with a localized electron in defect states. The 1.5% Sc^{3+} doping reduces these localized states appreciably, giving $y = 0.1\%$ (table 1), assuming they have spin $S = 1/2$. The lowest Sc d-states lie well above the bottom of the Ti 3d band on account of the smaller nuclear charge and are expected to be unoccupied. The main effect of Sc doping seems to be to reduce slightly the number of electrons in localized defect states and introduce further potential fluctuations.

V, Cr and Mn form the next group of dopants. If we assume they adopt a trivalent configuration in octahedral oxygen coordination, where they substitute for Ti, then these ions have $S = 1, 3/2$ and 2, respectively. Mn has the largest spin moment, so if any of the dopants exhibit spin-glass ordering, it should be Mn. The Mn-doped sample shows a paramagnetic Curie temperature of −1 K, but there is no sign of spin freezing in field-cooled or zero-field-cooled scans of the moment in 10 mT. We deduce that exchange coupling between dilute magnetic impurities in LSTO is very weak, as anticipated.

Finally, we discuss the group of dopant elements Fe, Co and Ni that exhibit ferromagnetic order. All three also show a Curie–Weiss upturn in their susceptibility. Setting aside Ni, where the moment is consistent with the presence of most of the nickel as a second phase of nickel metal, we focus on the Fe and Co materials. From the magnetization curves for Fe at 4 K (figure 5), it is obvious that only part of the iron orders ferromagnetically, while the rest remains paramagnetic. Cobalt behaves similarly. Fitting the iron data on figure 5 to a Brillouin function give a value of the concentration of paramagnetic iron of 90%, which is consistent with the Mössbauer analysis of the same sample (figure 9(b)) which gives around 80%. Even though a ratio of 0.37% Fe^{3+}/Fe^{2+}, as derived from the Mössbauer data, is compatible with the low temperature magnetization data, we have obtained the best fit for the same with only Fe^{2+} taken into account.

The ^{57}Fe Mössbauer spectra are quite informative. The ceramic sample shows only paramagnetic Fe^{3+} iron; there is no ferromagnetic moment and the magnetization curve is linear. The iron-doped nanoparticles all show small magnetic moments in the range 0.03–0.09 A m^2 kg^{-1}. The spectrum of the sample doped with natural iron is rather poorly resolved, showing only the paramagnetic doublets of Fe^{2+} and Fe^{3+}, but when the oxide is prepared with ^{57}Fe, two weak magnetic hyperfine patterns can be resolved in the room temperature spectrum. One, with 18% of the total absorption, is due to an antiferromagnetically ordered ferric oxide, most probably haematite with a little Ti substitution. The other, with 3% of the total absorption, has a hyperfine field of 33 T and an isomer shift of 0.00 mm s^{-1} relative to metallic iron, which are the parameters of iron metal itself. The small moment measured in this sample, 0.06 A m^2 kg^{-1}, corresponds to the moment expected if 5% of the dopant iron was metallic, which is consistent with what is observed in the Mössbauer spectrum. Iron metal has a moment of 220 A m^2 kg^{-1}. The breakdown of the iron content in this sample is summarized in table 4.

It must be emphasized that the magnetization curves in figure 5, after subtracting the component due to paramagnetic iron, do not exhibit the $M(H/T)$ scaling expected for isolated superparamagnetic particles. The curves show hysteresis which doubles between 300 and 4 K (figure 5), and the magnetization saturates readily in about 0.5 T, even at 300 K. The curves for the Co-doped material, shown in figure 6, are similar. The ferromagnetic metal cannot be present in the form of non-interacting nanoparticles. If small metallic

clusters are present, they must interact strongly, presumably via the conduction electrons of LSTO. Otherwise, micron-scale ferromagnetic particles might be present in these samples, but these would be scarce and difficult to detect.

For the Co-doped LSTO, the quantity of paramagnetic cobalt is deduced by fitting the 4 K magnetization curves to a constant ferromagnetic term plus a Brillouin function for $S = 3/2$. Assuming high spin Co^{2+} (the data are not compatible with low spin cobalt with $S = 1/2$), this gives $y = 92\%$. The ferromagnetic moment $\sigma = 0.3$ A m^2 kg^{-1} could be attributed to ferromagnetically ordered cobalt. Traces of antiferromagnetic CoO may possibly be present in the nanoparticles, which would increase the ferromagnetic moment per cobalt towards the value 170 A m^2 kg^{-1} for cobalt metal. We were unable to see any sign of cobalt in the x-ray diffraction patterns (but this was also true of iron metal, which turned out to be present, according to the Mössbauer spectrum). By analogy with iron and nickel, we think it is likely that cobalt metal nanoclusters are present in the Co-doped LSTO, but we cannot exclude the possibility that the material might be intrinsically a high temperature ferromagnet, as claimed [29–31].

Recently, a new model of charge transfer ferromagnetism (CTF) has been developed to explain how dilute magnetic oxides could possibly exhibit high temperature ferromagnetism [33, 36]. The widespread view that these materials are homogeneous dilute magnetic semiconductors (DMS) is unsustainable in view of the low doping levels and the strength of known exchange mechanisms. The CTF model envisages sparse Stoner ferromagnetism associated with defects, with a local density of states associated with structural defects, and a proximate charge reservoir. Electron transfer to or from the reservoir to the defect states may fill the defect states to the point where they split spontaneously, provided the Stoner criterion is satisfied. The ferromagnetism in the CTF model is therefore due to Stoner splitting of a network of defect states, which does not involve the whole sample. The proximate charge reservoir is the 3d dopant which can coexist in two different charge states such as Fe^{2+} and Fe^{3+}.

The defect states in nanoparticles and nanocrystalline ceramics are likely to be associated with the surfaces or grain boundaries. The fraction of surface or grain boundary sites is $f = 3a_0/r$, where r is the particle radius and $a_0 \approx 0.25$ nm is the cation–cation distance. In the present case, this fraction is $f \approx 10\%$. Metallic nanoparticles have a common Fermi energy for conduction electrons in bulk and surface states, so the relative energy change of the two would be f on electron transfer from one to the other. However, the characteristic wavelength on which it is possible to modulate the electron density is $2\pi/k_F$, which is ~0.1 nm in the present particles. We would only expect the charge transfer ferromagnetism mechanism to be effective at nearest-neighbour distances, with the defect potential being screened over longer lengths.

The transparency of the ceramic oxides (yellow colour) can be understood in the same way as for transparent conducting oxides such as SnO_2 or ITO. The energy gap E_g is greater than the optical photon range and d–d transitions in the conduction band have low probability.

In summary, the LSTO matrix for the ceramic samples can be regarded as a weakly correlated d-band metal, where the electrons are localized by potential fluctuations. The nanocrystalline material is more highly correlated, with long-lived charge fluctuations, which may be considered as a superposition of Ti^{3+} and Ti^{4+} charge states.

5. Conclusions

The undoped LSTO nanoparticles are diamagnetic with an estimated oxygen excess $\delta = 8\%$. Both undoped and Sc-doped nanoparticles contain a small concentration of order 0.1% of paramagnetic defect centres. When doped with V, Cr or Mn, there is an additional Curie law susceptibility which agrees with expectations for dilute substitutional impurities with negligible interatomic exchange interactions. For Fe, Co and Ni doping, where hysteretic ferromagnetism with a large remanence coexists with Curie law paramagnetism, the natural explanation is to attribute the ferromagnetism to inclusions of a secondary phase of ferromagnetic metal. There is direct evidence of this for Fe from Mössbauer spectra and for Ni from x-ray diffraction. Although we have no direct evidence, it is plausible to infer that the presence of metallic Co nanoparticles accounts for about a third of the cobalt in the Co-doped material. It is difficult to envisage charge transfer ferromagnetism in metallic LSTO nanoparticle materials where the screening length is less than the interatomic distance.

Acknowledgments

We are grateful to Peter Dunne and Robbie Gunning for the Mössbauer data and to Plamen Stamenov for useful discussions. The work was supported by Science Foundation Ireland as part of the MANSE project, and by the Thai Commission on Higher Education.

References

[1] Matsumoto Y, Murakami M, Shono T, Hasegawa T, Fukumura T, Kawasaki M, Ahmet P, Chikyow T, Koshihara S and Koinuma H 2001 *Science* **291** 854
[2] Coey J M D 2007 *Curr. Opin. Solid State Mater. Sci.* **10** 83
[3] Sundaresan A, Bhargavi R, Rangarajan N, Siddesh U and Rao C N R 2006 *Phys. Rev.* B **74** 161306
[4] Crespo P *et al* 2004 *Phys. Rev. Lett.* **93** 097204
[5] Carmeli I, Leitus G, Naaman R, Reich S and Vager Z 2003 *J. Chem. Phys.* **118** 10372
[6] Radovanovic P V and Gamelin D R 2003 *Phys. Rev. Lett.* **91** 157302
[7] Martinez B *et al* 2005 *Appl. Phys. Lett.* **86** 103113
[8] Zhang Z H *et al* 2009 *Nat. Nanotechnol.* **4** 523
[9] Straumal B B *et al* 2009 *Phys. Rev.* B **79** 205206
[10] Straumal B B *et al* 2008 *Acta Mater.* **56** 6246
[11] Fitzgerald C B *et al* 2004 *J. Appl. Phys.* **95** 7390
[12] Cabrera A F *et al* 2007 *Physica* B **398** 215
[13] Archer P I *et al* 2005 *J. Am. Chem. Soc.* **127** 14479
[14] Van Komen C *et al* 2008 *J. Appl. Phys.* **103** 07D141
[15] Thurber A, Reddy K M and Punnoose A 2009 *J. Appl. Phys.* **105** 07E706

[16] Bryan J D, Heald S M, Chambers S A and Gamelin D R 2004 *J. Am. Chem. Soc.* **126** 11640
[17] Thurber A *et al* 2007 *Phys. Rev.* B **76** 165206
[18] Sundaresan A, Bhargavi R, Rangarajan N, Siddesh U and Rao C N R 2006 *Phys. Rev.* B **74** 161306
[19] Bérardan D, Guilmeau E and Pelloquin D 2008 *J. Magn. Magn. Mater.* **320** 983
[20] Archer P I and Gamelin D R 2006 *J. Appl. Phys.* **99** 08M107
[21] Coey J M D, Mlack J T, Venkatesan M and Stamenov P 2010 *IEEE Trans. Magn.* at press
[22] Lawes G, Risbud A S, Ramirez A P and Seshadri R 2005 *Phys. Rev.* B **71** 045201
[23] Rao C N R and Deepak F L 2005 *J. Mater. Chem.* **15** 573
[24] Kaspar T C, Heald S M, Wang C M, Bryan J D, Droubay T, Shutthanandan V, Thevuthasan S, McCready D E, Kellock A J, Gamelin D R and Chambers S A 2005 *Phys. Rev. Lett.* **95** 217203
[25] Oschenbein S T *et al* 2009 *Nat. Nanotechnol.* **4** 681
[26] Coey J M D, Venkatesan M and Fitzgerald C B 2005 *Nat. Mater.* **4** 173
[27] Sunstrom J E, Kauzlarich S M and Klavins P 1992 *Chem. Mater.* **4** 346
[28] Tokura Y *et al* 1993 *Phys. Rev. Lett.* **70** 2126
[29] Zhao Y G *et al* 2003 *Appl. Phys. Lett.* **83** 2199
[30] Ranchal R, Bibes M, Barthe'le'my A and Bouzehouane K 2005 *J. Appl. Phys.* **98** 013514
[31] Wongsaprom K, Swatsitang E, Maensiri S, Srijaranai S and Seraphin S 2007 *Appl. Phys. Lett.* **90** 162506
[32] Wongnasprom K 2009 *PhD Thesis* Khon Kaen University, Thailand
[33] Coey J M D, Wongsaprom K, Alaria J and Venkatesan M 2009 *J. Phys. D: Appl. Phys.* **41** 134012
[34] Coey J M D 2010 *Magnetism and Magnetic Materials* (Cambridge: Cambridge University Press)
[35] Mott N F 1985 *Metal–Insulator Transitions* 2nd edn (London: Taylor and Francis)
[36] Coey J M D, Stamenov P, Gunning R D, Venkatesan M and Paul K 2010 *New J. Phys.* at press